# Nanoscale

This is an *Accepted Manuscript*, which has been through the Royal Society of Chemistry peer review process and has been accepted for publication.

*Accepted Manuscripts* are published online shortly after acceptance, before technical editing, formatting and proof reading. Using this free service, authors can make their results available to the community, in citable form, before we publish the edited article. We will replace this *Accepted Manuscript* with the edited and formatted *Advance Article* as soon as it is available.

You can find more information about *Accepted Manuscripts* in the **Information for Authors**.

Please note that technical editing may introduce minor changes to the text and/or graphics, which may alter content. The journal's standard **Terms & Conditions** and the **Ethical guidelines** still apply. In no event shall the Royal Society of Chemistry be held responsible for any errors or omissions in this *Accepted Manuscript* or any consequences arising from the use of any information it contains.

# Journal Name

## ARTICLE

# Defective ZnFe$_2$O$_4$ nanorods with oxygen vacancy for photoelectrochemical water splitting

Ju Hun Kim,[a] Youn Jeong Jang,[a] Jin Hyun Kim,[a] Ji-Wook Jang,[b] Sun Hee Choi,[c] and Jae sung Lee [*d]

One-dimensional zinc ferrite (ZnFe2O4) nanorod photoanode was prepared by a simple solution method on the F-doped tin oxide glass substrate. Thermal treatment under the hydrogen or vacuum atmosphere improved the photoelectrochemical water oxidation activity up to 20 times. The various physical characterizations revealed that the oxygen vacancies were created by the treatments in the near surface region, which increased donor density and passivated the surface states. Hydrogen treatment was more effective and it was important to find optimum treatment conditions to take advantage of the positive role of oxygen vacancy as a source of electron donors and avoid its negative effect as electron trap sites.

## 1. Introduction

Last decade has observed rapid progress in semiconductor-based photoelecrochemical (PEC) water splitting into hydrogen and oxygen as an eco-friendly method to convert solar energy to a storable and clean chemical energy. Among various semiconductors, metal oxides have received great attention as photoelectrodes due to their excellent durability, non-toxicity and earth abundance. However, there are only a limited number of metal oxides of a small band gap and proper band positions for solar water splitting such as Fe$_2$O$_3$, WO$_3$, BiVO$_4$, and TaON.[1-5] However even these materials have numerous limitations including insufficient optical band gap and poor charge mobility. Hence, we need to search for new photoelectrode materials that are able to absorb a large fraction of solar spectrum, and to develop strategies to improve their charge transfer properties.

In this regard, the spinel ferrites (MFe$_2$O$_4$) could be a class of promising candidate photoelectrode materials because they have attractive small band gaps around 2 eV, corresponding to a theoretical solar-to-hydrogen (STH) conversion efficiency close to 20%. In spite of the great potential, there have been only limited studies of these materials mainly as a supplementary component of composite photoelectrodes with

other semiconductor materials.[6-11] In those rare cases as a main component of photoelectrodes, they did not show any meaningful photoactivity. Their crystallization requires an extremely high temperature above 1000$^o$C and thus it is difficult to fabricate the photoelectrode on the heat-sensitive transparent conductive oxide substrate.[12-15] Thus, the first critical issue in utilizing these materials for PEC applications is to find a way to crystallize at mild temperatures.[15, 16] Next, formation of nanostructures[5] and extrinsic/intrinsic doping are common and fruitful approaches to improved conductivity of these materials.[17, 18] In particular, introduction of oxygen vacancies into metal oxides is a relatively new method to tune their optical and electronic properties for improved PEC activity. For instance, the band gap of TiO$_2$ was narrowed after thermal hydrogen treatment down to <2eV yielding dramatically increased photoactivity because of extended visible light absorption.[19-21] The majority carrier concentration and the stability of WO$_3$ were enhanced due to formation of substoichiometric WO$_{3-x}$ layer.[22]

Here we introduce the nanostructured ZnFe$_2$O$_4$ with oxygen vacancies formed on F-doped tin oxide (FTO) substrate as an active photoanode for PEC water splitting. Thus, one-dimensional (1-D) ZnFe$_2$O$_4$ nanorods are synthesized on FTO by an all-solution method and then annealed under hydrogen flow or an oxygen-poor condition to introduce oxygen vacancies. These post-treated ZnFe$_2$O$_4$ electrode increased PEC water oxidation activity dramatically by 15-20 times relative to as-prepared ZnFe$_2$O$_4$ electrode. The effects of the post-treatment were the increased majority carrier concentration and passivation of surface defects, which led to improved bulk and surface charge separation efficiencies. The oxygen vacancies formed by the treatments played dual roles of positive and negative effects on PEC water oxidation activity, *i.e.* a source of electron donor to increase the charge carrier

a. Department of Chemical Engineering, Pohang University of Science and Technology (POSTECH), Pohang 790-784, Korea
b. Institute for Solar Fuels, Helmholtz-Zentrum Berlin für Materialien und Energie GmbH, Hahn-Meitner-Platz 1, 14109 Berlin, Germany
c. Pohang Accelerator Laboratory (PAL),Pohang University of Science and Technology (POSTECH), Pohang 790-784, Korea
d. School of Energy and Chemical Engineering, Ulsan National Institute of Science and Technology (UNIST) Ulsan 689-798, Korea. E-mail: jlee1234@unist.ac.kr
e. Electronic Supplementary Information (ESI) available: XANES and EXAFS spectra, light harvesting efficiency, HR-SEM images, vacuum-treated ZnFe2O4, equivalent circuit model, Nyquist plots, and charge separation efficiencies. See DOI: 10.1039/x0xx00000x

density, or electron trap sites to provide charge recombination centres.

## 2. Experimental Section

### 2.1 Synthesis of ZnFe2O4 Nanorod Photoanode

The nanostructured $ZnFe_2O_4$ photoanode was fabricated on the FTO substrate by an all-solution method.[1, 14] First, amorphous β-FeOOH (iron oxyhydroxide) nanorod was grown on FTO glass (PECTM 8, 6~9 Ω, Pilkington) at 100 $^o$C by using a precursor solution containing 0.15M $FeCl_3 \cdot 6H_2O$ and $NaNO_3$ for 6 h, followed by rinsing with abundant deionized water to obtain yellow β-FeOOH nanorod. The 100 μL of 60mM $Zn(NO_3) \cdot 6H_2O$ aqueous solution was dropped on the β-FeOOH film. The wet electrode was transferred to a furnace which was already heated to 800$^o$C and annealed for 20min. During the annealing process, the β-FeOOH nanorods turned into $ZnFe_2O_4$ nanorods wrapped with excess ZnO layer. This unwanted ZnO skin was removed by soaking into a 1M NaOH solution for 12 h with stirring. The procedure resulted in pure $ZnFe_2O_4$ nanorods on FTO. To form defective oxygen vacancies of different concentrations, the electrode was subsequently treated under hydrogen, vacuum or air in a customized furnace. The vacuum treatment was carried out at $10 \times 10^{-3}$ torr in a vacuum furnace.

### 2.2 Characterization of Films

The samples were characterized by X-ray diffraction (XRD) with PW3040/60 X'pert PRO (PANalytical), using Cu-K α ( λ =1.54056Å) radiation, an accelerating voltage of 40 kV and an emission current of 30 mA. High-resolution scanning electron microscopy (SEM, HITACHI) was used to observe the morphology at UNIST Central Research Facilities (UCRF), Ulsan, Korea. The X-ray absorption fine structure (XAFS) measurements were conducted on beam line 7D of Pohang Accelerator Laboratory (PLS-II, 3.0 GeV) in Korea. The radiation was monochromatized using a Si(111) double crystal monochromator and the incident beam was detuned by 15% for harmonic rejection. The spectra for K-edges of Fe ($E_0$=7112 eV) were taken in a fluorescence mode at room temperature. The intensity of the incident beam was measured with a He-filled IC Spec ionization chamber and the fluorescence signal from the sample with a Passivated Implanted Planar Silicon (PIPS) detector. Helium gas was steadily flown into the sample chamber where the PIPS detector was attached, optimizing noises induced from scattering with atmospheric air. The obtained data were analyzed with Athena in the IFEFFIT 1.2.11 suite of software program. X-ray photoelectron spectroscopy (XPS) was carried out on a Thermo Fisher machine using Al Kα.

### 2.3 Photoelectrochemical Measurements

The PEC measurements were performed with a potentiostat (IviumStat, Ivium Technologies) using three electrode cell with $ZnFe_2O_4$ film, Ag/AgCl (3M NaCl), and Pt mesh as working, reference, and counter electrodes, respectively. An electrolyte of 1M sodium hydroxide purged with oxygen-free Ar gas was used for the measurements. All PEC experiments to obtain

photocurrent(J)-voltage(V) curve and electrochemical impedance spectra (EIS) were carried out under the 1 sun condition (100 mW/cm$^2$) by a solar simulator (91160, Oriel) with an AM 1.5G filter. The applied voltage was swept in the range of 0.6-1.9 $V_{RHE}$ with a scan rate of 10 mV/s. The EIS was measured at a DC potential of 1.23 $V_{RHE}$ and AC potential frequency range of 10000~0.1 Hz with an amplitude of 10 mV. Mott-Schottky analysis was performed by sweeping the range of 0.3-1.7 $V_{RHE}$ with AC frequency of 10 kHz and amplitude of 10 mV under dark condition.

## 3. Results and Discussion

### 3.1. Fabrication and Characterization of Defective $ZnFe_2O_4$ Nanorod Photoanodes

Yellow β-FeOOH nanorods were grown on FTO glass according to the reported procedure.[14] Then an aqueous Zn solution (60mM) was added dropwise onto the β-FeOOH thin film, which was heated at 800$^o$C for 20 min to obtain $ZnFe_2O_4$ nanorods covered with an excess ZnO layer. The ZnO layer was removed by soaking into a 1M NaOH solution to yield a pure $ZnFe_2O_4$ nanorod electrode. Then, various post treatments were conducted under various atmospheres to generate defective oxygen vacancies *i.e.* under hydrogen, vacuum or air. Through optimization experiments, it was determined that the post treatments of 2 h at 200 $^o$C gave the best photoactivity under all conditions. For convenience, the samples are denoted as as-prepared (annealed at 800 $^o$C), H200 (hydrogen-treated at 200 $^o$C), V200 (vacuum treated at 200 $^o$C) and A200 (air treated at 200$^o$C).

**Figure 1** shows XRD patterns of all the prepared electrodes. The peaks at 2θ=30$^o$ and 35.2$^o$ represent (220) and (311) crystal planes of the cubic spinel $ZnFe_2O_4$, respectively, with a space group of *Fd3m* (JCPDS card 01-089-4926) with no impurities such as ZnO or $Fe_2O_3$. (Figure S1)[14, 15] The post treatments did not change XRD patterns suggesting no change in bulk crystal structure unlike previous reports for hydrogen-treated $WO_3$ or $TiO_2$ photoelectrode.[21, 22] The samples treated at temperatures higher than 200 $^o$C in hydrogen and vacuum also showed no change in XRD patterns as discussed later.
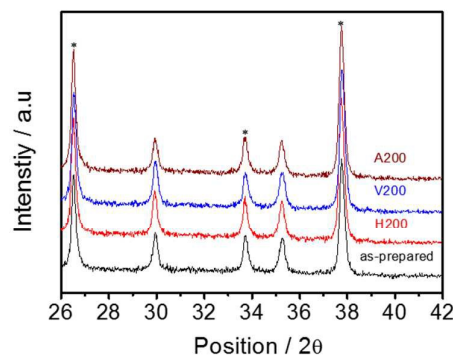


Figure 1. XRD of $ZnFe_2O_4$ annealed at 800$^o$C, the post-treated samples under hydrogen (H), vacuum (V) and air (A) atmosphere at 200$^o$C. (*= peaks from FTO. The peaks at 2θ=30$^o$ and 35.2$^o$ represent (220) and (311) crystal planes of the cubic spinel $ZnFe_2O_4$.)
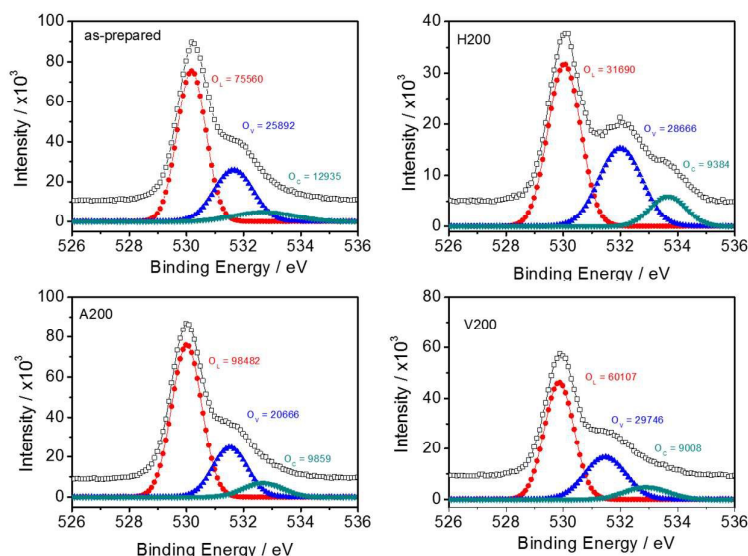
Figure 2. XPS spectra of O 1s electronic level of as prepared, H200, V200 and A200 electrodes.

Table 1. The relative ratio of O1s peak area and atomic percent of each element measured by XPS. ($N_d$=donor density obtained from Mott-Schottky plots in Figure 3d)

| Samples | Relative ratio of O1s peak areas | | | Relative Atomic percent (At.%) | | | $N_d$ |
|---------|-----------|-----------|----------------|-------|-------|-------|-------|
|         | Lattice ($O_L$) | Vacancy ($O_V$) | Chemisorb ($O_C$) | Zn 2p | Fe 2P | O1s | #/cm³ |
| as-prepared | 0.660 | **0.226** | 0.113 | 8.12 | 12.75 | 79.12 | 2.49E+18 |
| H200 | 0.454 | **0.411** | 0.135 | 8.32 | 18.19 | 73.47 | 1.27E+19 |
| V200 | 0.607 | **0.300** | 0.091 | 9.03 | 17.71 | 73.25 | 4.23E+18 |
| A200 | 0.763 | **0.160** | 0.076 | 7.15 | 13.00 | 79.84 | 1.92E+18 |

In order to investigate the structural changes in more detail, the X-ray absorption fine structure (XAFS) analysis was carried out. In Figure S2 of Electronic Supplimentary Information (ESI), Fe K-edge X-ray absorption near-edge structures (XANES) spectra of all samples are very close to each other indicating no change in electronic structure by hydrogen and vacuum treatments. If oxygen ($O^{2-}$) is removed from $ZnFe_2O_4$ lattice, the vacated site is taken by one or two free electrons for charge neutralization forming a donor level. The local surrounding should also be changed due to the free space induced by oxygen vacancy.[23] However, the Fe K-edge extended X-ray absorption fine structure (EXAFS) functions $k^2\chi$ (k) (k) for post-treated samples and their Fourier transforms show no particular difference compared with untreated $ZnFe_2O_4$ (Figure S3). Hence, both XRD and XAFS point out that there is no change in the bulk structure of $ZnFe_2O_4$. Hence, it is necessary to check the chemical states of the near surface regions before and after the post treatments.

X-ray photoelectron spectroscopy (XPS) of O 1s in **Figure 2** shows three peaks, which are located at 529.7±0.4, 531.6±0.5 and 532.3±0.7 eV. Each peak could be assigned to lattice $O^{2-}$ ions ($O_L$), the native defects of $O^{2-}$ vacancies ($O_V$), and $H_2O$ or –$CO_3$ bonds on the surface ($O_C$), respectively.[24-27] The

compositions of these species on the surface obtained from the relative peak area are presented in **Table 1**. The fraction of oxygen vacancies in as-prepared electrode was 0.226, which increased to 0.411 and 0.300 for the hydrogen-treated and vacuum treated samples, respectively. For the electrode annealed in the air (A200), the fraction is reduced to 0.160 by accepting more oxygen. Furthermore, the decreased relative oxygen atomic percent (from O1s) in post-treated electrodes is also observed. Thus, the post-treatment in the hydrogen or vacuum generates the oxygen vacancies in the near surface region of $ZnFe_2O_4$.

There was no change in light absorption capability of the $ZnFe_2O_4$ electrodes upon the post-treatment. Figure S4 exhibits almost the same light harvesting efficiency curves for all samples. The result is in contrast to large band gap $TiO_2$ that exhibits a narrowed band gap after the treatment inducing oxygen vacancies.[21] The SEM images of the samples are shown in Figure S5 and Figure S6. The pristine sample synthesized at 800°C (as-prepared) show the similar nanorod morphology like β-FeOOH, although the surface becomes smoother and the end of nanorods becomes a little rounder. Additional post-treatment did not alter the morphology either.[14]

# Journal Name

ARTICLE
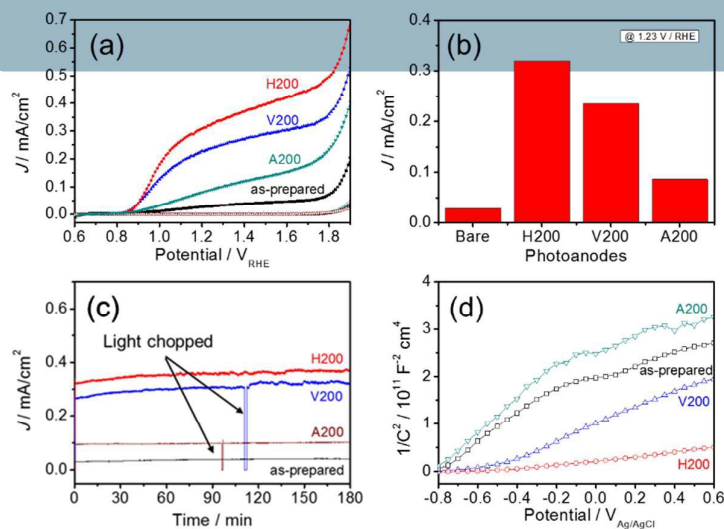


**Figure 3.** (a) *J-V* characteristics of ZnFe$_2$O$_4$ photoanodes before and after post-treatment under AM 1.5G illumination (100mW/cm$^2$) in 1M NaOH electrolyte. (scan rate =10mV/s). (b) The comparison chart of photocurrent at 1.23 V$_{RHE}$ under 1 Sun. (c) The stability test for continuous 3 h under 1 Sun illumination at 1.23 V$_{RHE}$. (d) The Mott-Schottky plots obtained at a frequency 1kHz and a amplitude of 0.01V under dark condition.

## 3.2. Photoelectrochemical Water Splitting

The photocurrent (J) *vs.* sweeping potential (V) curves were obtained from 0.6 to 1.9 V$_{RHE}$ in a 1M NaOH electrolyte under the 1-sun condition as shown in **Figure 3a.** As-prepared sample exhibits very little photocurrent (~15 μA/cm$^2$) at 1.23 V$_{RHE}$, but post-treated samples under hydrogen or vacuum show markedly improved photocurrents; H200 (320 μA/cm$^2$) > V200 (240 μA/cm$^2$) >> A200 (90 μA/cm$^2$) as shown in **Figure 3b**. The photocurrents remain stable for 3 h of continuous operation at 1.23 V$_{RHE}$. (**Figure 3c**). It is clear that hydrogen and vacuum treatments dramatically improve the PEC performance of ZnFe$_2$O$_4$ electrodes. To investigate the effect of these treatments, the electrical impedance measurement was conducted without light for Mott-Schottky analysis. In **Figure 3d**, all samples have n-type semiconductor property and H200 sample shows the highest donor density (N$_d$) according to the Mott-Schottky equation for the planar electrode model[28-32];

$$N_d = 2/(q\varepsilon_s \varepsilon_0) \times |d(1/C_{sc}^2)/dV|^{-1} \qquad (1),$$

where $\varepsilon_s, \varepsilon_0$ =dielectric constant of material and the permittivity of vacuum, q=electron charge, V=applied potential, and C$_{sc}$=depletion layer capacitance of semiconductor. The obtained donor densities in the last column of **Table 1** match well with the trend of induced oxygen vacancies from XPS in the same table. Thus we can deduce that the enhanced photo-activity originates from the increased majority carrier density due to oxygen vacancy.[1] Thus hydrogen reacts with the oxygen (O$_L$) in the lattice of ZnFe$_2$O$_4$ during the post-treatment to remove it as a water molecule and create an oxygen vacancy ($\ddot{V}_O$).[20] The process leaves two electrons behind that remain localized at the vacant site.

$$H_2 + O_L \rightarrow H_2O + \ddot{V}_O + 2e^- \qquad (2)$$
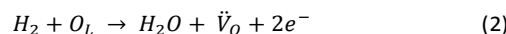
In contrast, oxygen removal from the vacuum-treated ZnFe$_2$O$_4$ electrode can be described by the following equilibrium.

$$O_L \rightleftharpoons 1/2O_{2(g)} + \ddot{V}_O + 2e^-; \text{K} \qquad (3)$$
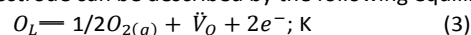
Then the concentration of oxygen vacancies [V$_o$] becomes;

$$[\ddot{V}_O] = Kn^{-2}[O_2]^{-1/2} \qquad (4)$$

where n is the electron density and [O$_2$] is the oxygen pressure of the treatment chamber. This equation indicates that oxygen-depleted vacuum condition also produces oxygen vacancies.[20] Therefore, the difference in photo-activity between H200 and V200 samples despite of the same temperature and time of the post-treatment is related with the different mechanisms of oxygen vacancy formation as depicted in **Scheme 1,** and obviously hydrogen treatment is more effective to generate oxygen vacancies.
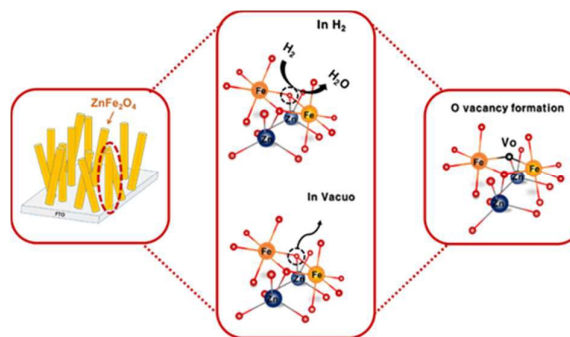


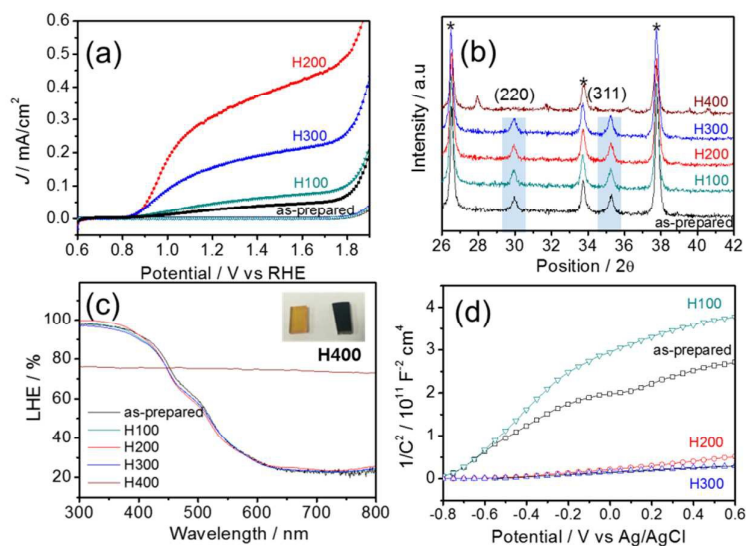Scheme 1. Different mechanisms of generating oxygen vacancies by post treatments under hydrogen or vacuum conditions.

Figure 4. Hydrogen-treated $ZnFe_2O_4$ photoanodes at different temperatures: (a) J-V characteristics under 1 sun (100 mW/cm²) in 1M NaOH electrolyte. (scan rate =10 mV/s). (b) XRD patterns (* = peaks from FTO). (c) Light harvesting efficiency (LHE). Inset shows optical images of H200 and H400 electrodes. (d) The Mott-Schottky plots.

It should be noted in **Figure 3d** that the as-prepared electrode (and A200 electrode to a lesser degree) shows a slope transition in the Mott-Schottky plot. It is usually indicative of Fermi level pinning associated with a high density of the surface trapped states. When a large amount of the trap sites exist on the top layer of semiconductor, the non-negligible potential drop is generated at the interface of electrolyte and semiconductor. This Fermi level pinning contributes a negative effect to charge separation due to reduced band bending.[33, 34] These unwanted defect states such as dangling bonds or lattice disorders may be generated after etching ZnO layer on $ZnFe_2O_4$. However the slope transition disappears for the electrodes treated under hydrogen and vacuum at 200°C because the density of the surface trapping sites is reduced. The presence of the slope transition also makes the determination of the flat band potential ($V_{fb}$) from Mott-Schottky plot less reliable. In any case, the results indicate that surface properties are also influenced by the thermal treatment.

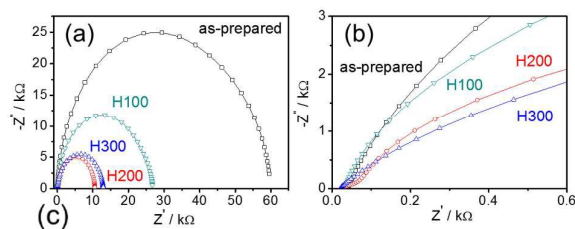### 3.3. Roles of Oxygen Vacancy: Donor Source *vs*. Trap Sites

As a donor source, the oxygen vacancies bring increased majority carrier concentration and change the charge transport properties such as mobility or resistance. However, the excess donor level could provide a negative effect by trapping the photo-induced electron and hole pair. The charge transfer in defective $ZnFe_2O_4$ nanorod is represented in **Scheme 2**. With a proper level of the oxygen vacancy, the transport of photo-induced charges is facilitated by the increased majority carrier concentration without serious recombination. However, the excessive oxygen vacancies become the recombination center by trapping the photo-

induced electrons that recombine with holes.[35] Thus, the optimum level of the oxygen vacancies in defective $ZnFe_2O_4$ is determined from the balance between their dual roles as a donor source and the trap sites.

The concentration of oxygen donor density was controlled by varying hydrogen treatment temperatures. As shown in **Figure 4a**, H200 electrode yields the highest photocurrent and H300 shows the decreased photocurrents. The H400 electrode shows the color change to black and no photocurrents, indicating deep reduction to metallic states. Except for this H400 electrode, the other hydrogen-treated electrodes show no change in crystal structure as seen by XRD patterns in **Figure 4b**, and absorption property as seen by light harvesting efficiency (LHE) in **Figure 4c**. The Mott-Schottky plot in **Figure 4d** shows that the donor density ($N_d$) of H300 (2.82E+19) is *ca*. 2 times larger than that of H200 (1.27E+19), but the photocurrent is smaller by a factor of *ca*. 2. The oxygen vacancy is an ionized donor atom of positive charge, and as the more oxygen vacancies are generated near the surface, the more positive charges are accumulated on the surface. The photo-generated electrons are more easily recombined with these positives charges or remaining electrons formed when generating oxygen vacancies may recombine with photo induced holes. As a result, the photocurrent is reduced in spite of increased donor densites. The electrodes treated under vacuum also show the same tendency as in Figure S8, although the difference between different treatment temperatures is smaller than the case of hydrogen treatment. The V400 electrode shows only slightly decreased photocurrents and higher anodic onset potential. The difference could be understood by different formation mechanisms between the two conditions as discussed earlier.
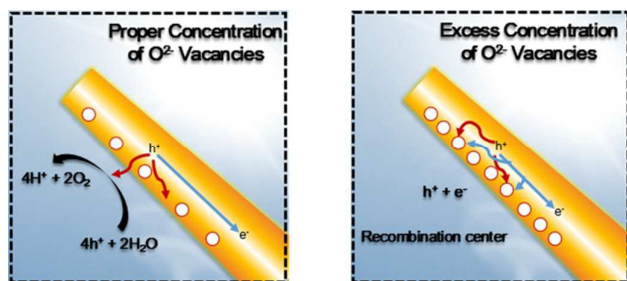
Scheme 2. The photo-induced charge transfer in a defective $ZnFe_2O_4$ nanorod with proper and excess concentrations of oxygen vacancies.



Figure 5. (a) The Nyquist plots of the $ZnFe_2O_4$ photoanodes treated with hydrogen at various temperatures and (b) the magnified plot. (c) Parameters extracted from fitting the data to a two-RC circuit model in Figure S9.

| (R/Ω) (CPE/ F) | Rs | R1 CPE 1 | R2 CPE 2 |
|---|---|---|---|
| as-prepared | 39.1 | 44888 $1.76 \times 10^{-11}$ | 14964 $2.51 \times 10^{-5}$ |
| H100 | 32.57 | 23712 $1.05 \times 10^{-11}$ | 3000 $1.67 \times 10^{-5}$ |
| H200 | 17.35 | 10455 $1.25 \times 10^{-6}$ | 64.2 $6.07 \times 10^{-6}$ |
| H300 | 19.75 | 12830 $1.0 \times 10^{-6}$ | 100 $2.5 \times 10^{-6}$ |

In **Figure 5,** the electrochemical impedance measurements under illumination at 1.23 $V_{RHE}$ were performed in order to understand the overall charge transfer. The Nyquist plots of hydrogen treated samples were best fitted to a two-RC circuit model in Figure S9. Although the Nyquist plots show only the single circle for all electrodes, the Bode plots indicate the presence of two peaks and the chi-squared values indicating goodness of fit is also shown reasonable ($10^{-4}$).

In the model, $R_s$ is the series resistance of electrolyte, FTO resistance and external contact. The first RC circuit ($R_{bulk}$, $C_{sc}$) is considered as internal resistance and capacitance of depletion region in the bulk of $ZnFe_2O_4$ and the charge transfer resistance ($R_{ct}$) and double layer capacitance, Helmholtz capacitance ($C_H$) are observed at the interface between semiconductor and electrolyte as another RC circuit in the proposed electrical configuration model. Given that most difficult electronic process takes place at $ZnFe_2O_4$||electrolyte, the low frequency response is assigned to this process.[1, 14, 36] This charge transfer resistance is greatly reduced upon hydrogen treatment up to 200°C (H200 electrode), and then increases again at higher temperature (H300). This trend is completely consistent with the PEC performance of the

electrodes. On the other hands, RC unit in the high frequency range is assigned to the semiconductor bulk that includes $R_{sc}$ and $C_{sc}$. This resistance also shows the minimal $R_{sc}$ and maximal $C_{sc}$ for H200 electrode. Similar results were obtained for vacuum treated $ZnFe_2O_4$ electrodes as summarized in Figure S10. Hence, we can conclude that the formation of oxygen vacancy improves the PEC performance by improving charge transfer properties of the $ZnFe_2O_4$ electrodes.



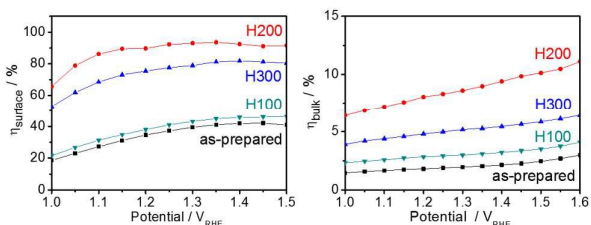Figure 6. Efficiency of interfacial charge separation ($\eta_{surface}$) and bulk charge separation ($\eta_{bulk}$) of pristine and hydrogen-treated photoanodes.

A more quantitative analysis to understand the charge separation efficiency was conducted by photo-oxidation of $H_2O_2$ as a hole scavenger.[37] The details of the analysis are provided in Figure S11, and the results are summarized in **Figure 6** as the efficiency of interfacial charge separation ($\eta_{surface}$) for all samples. The $\eta_{surface}$ was calculated by dividing the photocurrent from water oxidation by the photocurrent from $H_2O_2$ oxidation, because practically $\eta_{surface}$ = 1 for $H_2O_2$ photo-oxidation. Thus $\eta_{surface}$ value of the electrode treated by hydrogen at 200°C (H200) is the highest above 90%. Also, bulk charge separation efficiency ($\eta_{bulk}$) was calculated by dividing the photocurrent measured with $H_2O_2$ in electrolyte by the total absorbed photocurrent density ($J_{abs}$).[38] As shown in **Figure 6**, the values are low at 1-2% for as-prepared electrode, which increases to *ca*. 10% upon post hydrogen treatment at 200°C. Hence, improvement in $\eta_{surface}$ by passivation of surface trap sites seems more significant than improved $\eta_{bulk}$ by increased charge carrier density. Qualitatively similar results were obtained for vacuum treated $ZnFe_2O_4$ electrodes as summarized in Figure S11. But the effects in general are not as good as the hydrogen treatment

These observations demonstrate that the post thermal treatment under hydrogen or oxygen-deficient vacuum has profound effects by creating oxygen vacancies in $ZnFe_2O_4$ lattice. Thus the treatment under optimal condition increases the donor density by generating electrons for charge neutralization. It also passivates surface trap sites such as lattice disorder or dangling bonds. These effects lead to improved PEC performance of water oxidation by improving charge separation efficiencies at the semiconductor-electrolyte interface ($\eta_{surface}$) as well as in the bulk ($\eta_{bulk}$). Hydrogen treatment is more effective in all aspects and it is important to find optimum treatment condition to take advantage of the role of oxygen vacancy as a source of donors and avoid its negative effect as electron trap sites

　　　　　　　　　　　　　　　　　　　　　　　　　　　　　　　**ARTICLE**

## 4. Conclusion

One dimensional $ZnFe_2O_4$ nanorod photoanode for photoelectrochemical water splitting was successfully fabricated on FTO substrate by a facile solution method. This as-synthesized electrode exhibited little PEC activity under 1-sun illumination. However the thermal treatment under hydrogen and vacuum atmosphere gave drastically increased photocurrents compared to as-prepared or oxygen-treated $ZnFe_2O_4$ electrode. The various physical and electrochemical characterization demonstrates that the oxygen vacancies are generated near the surface of $ZnFe_2O_4$, and the electron density increases for charge neutralization. In addition, the surface states related with negative potential drop due to Fermi level pinning are passivated. Hydrogen treatment is more effective and it is important to find optimum treatment condition to take advantage of the role of oxygen vacancy as a source of donors and avoid its negative effect as electron trap sites. As a result, hydrogen-treated $ZnFe_2O_4$ electrode at $200^oC$ demonstrates ~ 20 times higher PEC activity of water oxidation than as-synthesized or oxygen treated electrodes by improving charge separation efficiencies both at the semiconductor-electrolyte interface as well as in the bulk.

## Acknowledgements

## References

1.　J. Y. Kim, G. Magesh, D. H. Youn, J.-W. Jang, J. Kubota, K. Domen and J. S. Lee, *Sci. Rep.*, 2013, **3,** 2681.
2.　W. J. Jo, J.-W. Jang, K.-j. Kong, H. J. Kang, J. Y. Kim, H. Jun, K. P. S. Parmar and J. S. Lee, *Angew. Chem. Int. Ed.*, 2012, **51**, 3147-3151.
3.　F. F. Abdi, L. Han, A. H. M. Smets, M. Zeman, B. Dam and R. van de Krol, *Nat Commun*, 2013, **4,** 2195.
4.　K. Sivula, F. Le Formal and M. Grätzel, *ChemSusChem*, 2011, **4**, 432-449.
5.　F. E. Osterloh, *Chem. Soc. Rev.*, 2013, **42**, 2294-2320.
6.　S. Boumaza, A. Boudjemaa, A. Bouguelia, R. Bouarab and M. Trari, *Applied Energy*, 2010, **87**, 2230-2236.
7.　J. Cao, J. Xing, Y. Zhang, H. Tong, Y. Bi, T. Kako, M. Takeguchi and J. Ye, *Langmuir*, 2013, **29**, 3116-3124.
8.　Y. Hou, X.-Y. Li, Q.-D. Zhao, X. Quan and G.-H. Chen, *Adv. Funct. Mater.*, 2010, **20**, 2165-2174.
9.　E. S. Kim, N. Nishimura, G. Magesh, J. Y. Kim, J.-W. Jang, H. Jun, J. Kubota, K. Domen and J. S. Lee, *J. Am. Chem. Soc.*, 2013, **135**, 5375-5383.
10.　K. J. McDonald and K. S. Choi, *Chem. Mater.*, 2011, **23**, 4863-4869.
11.　A. Sheikh, A. Yengantiwar, M. Deo, S. Kelkar and S. Ogale, *Small*, 2013, **9**, 2091-2096.
12.　R. Dom, R. Subasri, N. Y. Hebalkar, A. S. Chary and P. H. Borse, *RSC Advances*, 2012, **2**, 12782-12791.
13.　S. Ida, K. Yamada, T. Matsunaga, H. Hagiwara, Y. Matsumoto and T. Ishihara, *J. Am. Chem. Soc.*, 2010, **132**, 17343-17345.
14.　J. H. Kim, J. H. Kim, J.-W. Jang, J. Y. Kim, S. H. Choi, G. Magesh, J. Lee and J. S. Lee, *Adv. Energy. Mater.*, 2015, **5**, 1401933.
15.　A. A. Tahir and K. G. U. Wijayantha, *J. Photochem. Photobiol. A* 2010, **216**, 119-125.
16.　J. Cao, T. Kako, P. Li, S. Ouyang and J. Ye, *Electrochem. Commun.*, 2011, **13**, 275-278.
17.　K. P. S. Parmar, H. J. Kang, A. Bist, P. Dua, J. S. Jang and J. S. Lee, *ChemSusChem*, 2012, **5**, 1926-1934.
18.　G. Wang, Y. Ling and Y. Li, *Nanoscale*, 2012, **4**, 6682-6691.
19.　Y. H. Hu, *Angew. Chem. Int. Ed.*, 2012, **51**, 12410-12412.
20.　X. Pan, M.-Q. Yang, X. Fu, N. Zhang and Y.-J. Xu, *Nanoscale*, 2013, **5**, 3601-3614.
21.　G. Wang, H. Wang, Y. Ling, Y. Tang, X. Yang, R. C. Fitzmorris, C. Wang, J. Z. Zhang and Y. Li, *Nano Lett.*, 2011, **11**, 3026-3033.
22.　G. Wang, Y. Ling, H. Wang, X. Yang, C. Wang, J. Z. Zhang and Y. Li, *Energy Environ. Sci.* 2012, **5**, 6180-6187.
23.　C. E. Rodríguez Torres, G. A. Pasquevich, P. M. Zélis, F. Golmar, S. P. Heluani, S. K. Nayak, W. A. Adeagbo, W. Hergert, M. Hoffmann, A. Ernst, P. Esquinazi and S. J. Stewart, *Phys. Rev. B*, 2014, **89**, 104411.
24.　M. M. Can, S. I. Shah, M. F. Doty, C. R. Haughn and T. Fırat, *J. Phys. D: Appl. Phys.*, 2012, **45**, 195104.
25.　J. Gan, X. Lu, J. Wu, S. Xie, T. Zhai, M. Yu, Z. Zhang, Y. Mao, S. C. I. Wang, Y. Shen and Y. Tong, *Sci. Rep.* 2013, **3**, 1021.
26.　Y. Zhao, G. Dong, L. Duan, J. Qiao, D. Zhang, L. Wang and Y. Qiu, *RSC Advances*, 2012, **2**, 5307-5313.
27.　R. S. Lubna, A. Bakhtyar, Z. Hao, W. G. Wang, Y. Q. Song, H. W. Zhang, S. I. Shah and J. Q. Xiao, *J. Phys.: Condens. Matter*, 2009, **21**, 486004.
28.　I. Cesar, K. Sivula, A. Kay, R. Zboril and M. Grätzel, *J. Phys. Chem. C*, 2009, **113**, 772-782.
29.　H. K. Dunn, J. M. Feckl, A. Muller, D. Fattakhova-Rohlfing, S. G. Morehead, J. Roos, L. M. Peter, C. Scheu and T. Bein, *Phys. Chem. Chem. Phys,*, 2014, **16**, 24610-24620.
30.　Y. Ling, G. Wang, D. A. Wheeler, J. Z. Zhang and Y. Li, *Nano Lett.*, 2011, **11**, 2119-2125.
31.　Y. Ling, G. Wang, J. Reddy, C. Wang, J. Z. Zhang and Y. Li, *Angew. Chem.*, 2012, **124**, 4150-4155.
32.　M. Zhong, Y. Li, I. Yamada and J.-J. Delaunay, *Nanoscale*, 2012, **4**, 1509-1514.
33.　J.-C. Chou, S.-A. Lin, C.-Y. Lee and J.-Y. Gan, *J. Mater. Chem. A*, 2013, **1**, 5908-5914.
34.　X. Yang, C. Du, R. Liu, J. Xie and D. Wang, *J. Catal.*, 2013, **304**, 86-91.
35.　S. Shen, J. Jiang, P. Guo, C. X. Kronawitter, S. S. Mao and L. Guo, *Nano Energy*, 2012, **1**, 732-741.
36.　T. Lopes, L. Andrade, F. Le Formal, M. Gratzel, K. Sivula and A. Mendes, *Phys. Chem. Chem. Phys*, 2014, **16**, 16515-16523.
37.　H. Dotan, K. Sivula, M. Gratzel, A. Rothschild and S. C. Warren, *Energy Environ. Sci.* 2011, **4**, 958-964.
38.　H. W. Jeong, T. H. Jeon, J. S. Jang, W. Choi and H. Park, *J. Phys. Chem. C*, 2013, **117**, 9104-9112.